Gas-Phase Oxidation

Showcasing Zhenyu Sun's research at Department of Chemistry and Biochemistry, Ruhr University Bochum, Universitätsstraβe 150, 44801 Bochum, Germany.

Title: High-quality functionalized few-layer graphene: facile fabrication and doping with nitrogen as a metal-free catalyst for the oxygen reduction reaction

We demonstrate a facile, highly efficient and mild covalent functionalization of graphene using HNO_3 vapour. This results in functionalized few-layer graphene (FLG) that is high in both quantity and quality. It allows for further doping for applications, for example with nitrogen as a metal-free catalyst in the oxygen reduction reaction.

As featured in:

Journal of
Materials Chemistry A
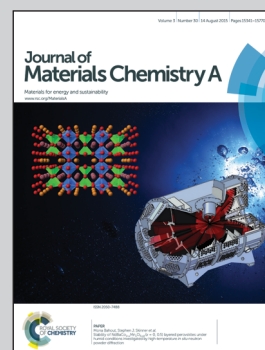
Materials for energy and sustainability
www.rsc.org/MaterialsA

ROYAL SOCIETY
OF CHEMISTRY

www.rsc.org/MaterialsA

High-quality functionalized few-layer graphene: facile fabrication and doping with nitrogen as a metal-free catalyst for the oxygen reduction reaction†

Zhenyu Sun,*[abcd] Justus Masa,[a] Philipp Weide,[b] Simon M. Fairclough,[c] Alex W. Robertson,[e] Petra Ebbinghaus,[f] Jamie H. Warner,[e] S. C. Edman Tsang,[c] Martin Muhler[b] and Wolfgang Schuhmann[a]

Functionalization of graphene is fundamental to facilitating its processing and offers a wide scope for advanced applications. Here we demonstrate a facile, highly efficient and mild covalent functionalization of graphene using HNO_3 vapour. This results in functionalized few-layer graphene (FLG) that is high in both quantity and quality. We fully characterized the structure and defect level of functionalized FLG by X-ray photoelectron spectroscopy, high-resolution transmission electron microscopy and Raman spectroscopy. The results from this analysis show the tunability of the surface oxygen functionalities of FLG achieved through controlling the oxidation temperature without affecting the major intrinsic properties of graphene. This allows for further doping for applications, for example with nitrogen as a metal-free catalyst in the oxygen reduction reaction.

1. Introduction

There have been intense research efforts recently focused on the functionalization of graphene to help facilitate processing and enable advanced applications to be realised.[1–3] Two strategies are well established and applied to the chemistry of graphene, akin to that of carbon nanotubes: (1) covalent functionalization *via* oxidation,[4] hydrogenation,[5] diazonium reaction,[6] n-type or p-type chemical doping[7,8] and (2) non-covalent functionalization with solvents,[9,10] surfactants,[11,12] polymers[13,14] or biomolecules.[15] Covalent modification is of particular interest as it allows fine tuning of the electronic and optical properties of the two-dimensional structure, offering potential for graphene manipulation and further development of novel and multifunctional materials. Currently, the most common approach is

the wet chemical oxidation of graphite with an excess of strongly oxidizing reagents (*e.g.*, HNO_3, H_2SO_4, $KMnO_4$), resulting in oxygen functionalities such as epoxide, carboxy, or hydroxy moieties.[16] However, in addition to the tedious multi-step processes involved, toxic gases (*e.g.*, NO_2, N_2O_4, and/or ClO_2) are potentially generated causing safety concerns and environmental issues. Another major disadvantage is the severe disruption of the π system, leading to extensive degradation of graphene's electronic structure. A large number of irremediable holes and sp^3 defects with an average distance of 1–2 nm are formed as a result of the aggressive oxidation, which significantly hinders applications that require high-quality functionalized graphene. Aside from these drawbacks, interfering heteroatomic species such as S, or metal-containing impurities (K and/or Mn) may be covalently bound or strongly physisorbed to graphene oxide (GO), thus complicating further processing.[17] Indeed, we recently showed that the presence of trace metal residues can profoundly alter the electrocatalytic properties of the catalyst.[18] Therefore, it is important to develop new ways that enable an effective surface modification, while retaining the inherent properties of graphene.

Herein, we show that high-quality functionalized few-layer graphene (FLG) can be produced on a large scale through a mild, but effective, gas-phase oxidation protocol using HNO_3 vapour. This method has aesthetic appeal due to its simplicity and ease of handling, and also avoids the adventitious introduction of foreign metal atoms. Importantly, controlling the oxidation temperature allows the surface oxygen functionalities

[a]*Analytical Chemistry Center for Electrochemical Sciences (CES), Ruhr-Universität Bochum, 44780 Bochum, Germany. E-mail: zhenyus@iccas.ac.cn; Fax: +49 234 3214115*

[b]*Laboratory of Industrial Chemistry, Ruhr-Universität Bochum, 44780 Bochum, Germany*

[c]*Department of Chemistry, University of Oxford, OX1 3QR, UK*

[d]*State Key Laboratory of Chemical Resource Engineering, Beijing University of Chemical Technology, Beijing 100029, China*

[e]*Department of Materials, University of Oxford, OX1 3PH, UK*

[f]*Max-Planck-Institut für Eisenforschung GmbH, Max-Planck-Str. 1, 40237 Düsseldorf, Germany*

to be readily tuned whilst preserving the majority of the intrinsic properties of graphene. Moreover, we show that the functionalized FLG can be further doped with nitrogen resulting in a metal-free catalyst for oxygen reduction.

2. Experimental

2.1. Materials

All chemicals used in this work were of analytical grade and used as supplied. N-Methyl-2-pyrrolidinone (product number 328624) (NMP) and nitric acid (product number 30709) were purchased from Sigma-Aldrich. Graphite powder (product number 332461) was also acquired from Sigma-Aldrich and used without further treatments.

2.2. Liquid-phase exfoliation of graphite to make graphene

Pristine layered graphite flakes were used as starting materials for graphene exfoliation. Graphene dispersions were prepared by adding graphite to 400 mL NMP (500 mL round-bottom flask) with the aid of bath ultrasonication (Bandelin Sonorex, 35 kHz), a technique applied to accelerate exfoliation.[9] After 48 h of ultrasonication, the dispersions were left to stand overnight to allow any unstable graphite aggregates to form and were subsequently centrifuged (ROTOFIX 32A). After centrifugation at 3000 rpm for 30 min, the top two-thirds of the dispersions were gently extracted by pipetting. Few-layer graphene powder was obtained by vacuum filtration of the centrifuged dispersions onto porous nylon membranes (Whatman, 0.2 μm pore size, 47 mm membrane diameter) followed by drying at 60 °C overnight.

2.3. Functionalization of few-layer graphene

A simple gas-phase oxidation strategy was adapted in this procedure. Typically, the filtered few-layer graphene flakes were functionalized using a nitric acid vapor at varying temperatures for 13 h. After cooling, the sample was dried at 60 °C overnight, obtaining oxidized FLG (OFLG). For doping of OFLG with nitrogen, 50 mg of the OFLG was loaded into a tubular quartz reactor, and 10 vol% NH_3 in He was introduced at 400 °C for 6 h with a flow rate of 25 sccm.

2.4. Characterization

The structure and quality of the functionalized few-layer graphene were evaluated by multiple characterizations, including X-ray diffraction (XRD), X-ray photoelectron spectroscopy (XPS), scanning electron microscopy (SEM), transmission electron microscopy (TEM) and Raman spectroscopy. XRD was performed with a D/MAX-RC diffractometer operated at 30 kV and 100 mA with Cu Kα radiation. XPS measurements were carried out in an ultra-high vacuum (UHV) setup equipped with a monochromatic Al Kα X-ray source ($h\nu = 1486.6$ eV), operated at 14.5 eV and 30.5 mA. The base pressure in the measurement chamber was maintained at about 5×10^{-10} mbar. The high-resolution spectra were carried out in the fixed transmission mode with pass energy of 200 eV, resulting in an overall energy resoluti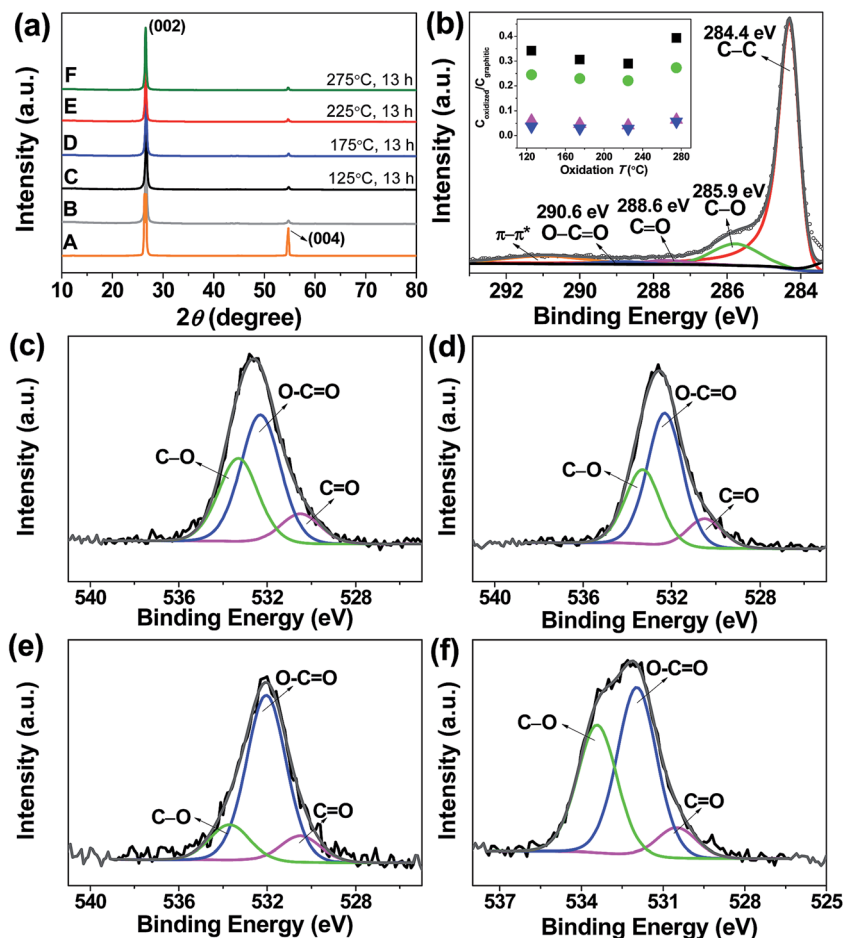on of 0.6 eV. A flood gun was applied to compensate for the charging effects. The CasaXPS software with a Gaussian–Lorentzian product function and Shirley background subtraction was used for peak deconvolution. SEM observations were carried out using a field emission microscope (FEI Quanta 600 FEG) operated at 20 kV and equipped with an energy-dispersive X-ray spectrometer. Standard TEM was using a JOEL 2100 running at 80 kV. HRTEM images were taken using a double aberration corrected JOEL 2200MCO TEM with CEOS third-order probe and image aberration correctors operated at 80 kV. The images were processed by applying a low pass FFT filter on the images, and regions of amorphous carbon were identified by masking and subtracting the crystalline graphene identified through the FFT from the image.[19] TEM samples were prepared by pipetting a few milliliters of the dispersion in ethanol onto holey carbon mesh grids (400 mesh). Raman spectra of graphene films and graphite powder were collected with a Horiba Jobin Yvon LabRam 2 confocal Raman microscope with a HeNe laser excitation at 633 nm (1.96 eV) with a power of 3.7 mW. Deposited thin films were prepared by vacuum filtration of the dispersions in NMP onto porous nylon membranes (Whatman, 0.2 μm pore size, 47 mm membrane diameter) and dried at room temperature. Measurements were taken with 5 s of exposure time using a long working distance objective of 50-fold magnification and aperture 0.5 yielding a beam diameter of ~600 nm in the focus. The peak maximum intensity ratio I_D/I_G was obtained by taking the peak intensities following baseline corrections to remove residual fluorescence.

3. Results and discussion

To gain insight into the structure and quality of the obtained flakes, a number of characterization methods were applied (vide infra). The X-ray diffraction (XRD) patterns of the resultant samples, in Fig. 1a, indicate good crystallinity of the hexagonal structure regardless of the oxidation up to 275 °C. The diffraction peaks at ~26.8 and ~54.8° in all traces are attributed to the (002) and (004) reflections of the graphite structure, respectively.[10,13,14] The two peaks in traces B–F in Fig. 1a, appear at the same position as those in trace A, which suggests that the graphite lattice was retained after the chemical treatment. No pronounced peak at 10°, characteristic of GO corresponding to a basal spacing of 0.85 nm, was found. A significant weakening in the intensity of the (004) reflection, relative to graphite, occurred in all cases, which supports the formation of randomly stacked few-layer graphene.[10,13,14] Fig. S1† shows the UV-vis spectra of pristine FLG and oxidised FLG. A strong peak at about 269 nm was observed in both cases which is due to the conjugated aromatic domains in the graphitic structure.[12] However, we did not see any pronounced absorption peak at 230 nm attributable to conjugated ketones or dienes typical for GO.[17] This suggests that the chemical structure of our oxidised FLG is distinct from the conventional GO. X-ray photoelectron spectroscopy (XPS) analysis was further employed to probe the surface oxygen species in the samples (Fig. 1b–f and S2†). A dominant C 1s peak at 284.4 eV, assigned to sp^2 graphitic carbon, was observed in all cases (Fig. 1b and S2b–d†). Carbon singly bound to oxygen in phenols and ethers (i.e. C–O) at

This journal is © The Royal Society of Chemistry 2015

J. Mater. Chem. A, 2015, 3, 15444–15450 | 15445

Fig. 1 (a) XRD patterns of starting graphite (trace A), pristine FLG (trace B) and functionalized FLG obtained at varying temperatures (traces C–F). (b) C 1s XPS spectrum of the functionalized FLG produced at 225 °C. Inset: molar ratio of C singly bound to oxygen (♦), carbon doubly bound to oxygen (▲), carbon bound to two oxygen atoms (▼) and the sum of the three C (■) to graphitic C as a function of oxidation T. O 1s XPS spectra of functionalized FLG at (c) 125 °C, (d) 175 °C, (e) 225 °C and (f) 275 °C.
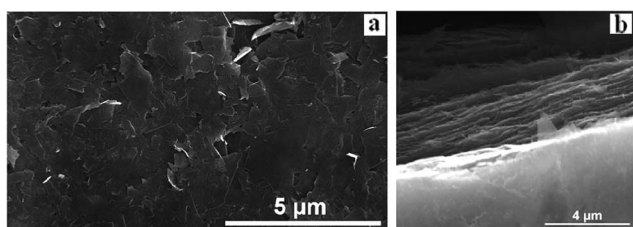
Fig. 2 SEM images of a film formed by vacuum filtration of the OFLG (obtained at 225 °C) dispersion in NMP: (a) the surface and (b) edge of the film. In addition to small flakes of several hundred nanometers, large sheets with dimensions of up to 5 μm in length were detected. The edge of the film consists of interconnected flakes showing a well-defined layered morphology.

285.9 eV, carbon doubly bound to oxygen in ketones and quinones (*i.e.* C=O) at 287.6 eV, carbon bound to two oxygen atoms in carboxyls, carboxylic anhydrides and esters (*i.e.* –COO) at 288.9 eV, and the characteristic shake-up line of aromatic compounds at 290.9 eV ($\pi \rightarrow \pi^*$ transition) may also contribute.[20] We further estimated the ratio of C bound to varying O species and graphitic C (sp^2), as shown in the inset of Fig. 1b. It shows that the FLG functionalized at 125 °C contains 25% oxidised C and 75% graphitic C. All four ratios tended to decrease with the oxidation temperature below 275 °C suggesting that the removal of metastable O species is predominant, rather than the introduction of new O moieties during the treatment. However, an increase of the ratios was observed at 275 °C indicative of higher amounts of O containing functional groups. Despite this, we note that the oxidation level at 275 °C (28% oxidised C and 72% graphitic C) is still much lower than the one reported for GO in literature (69% oxidised C and 31% graphitic C).[21] Deconvolution of the O 1s spectrum manifested three peaks at 530.5, 532.4, 533.4 eV indicating the presence of various oxygen-containing functional groups with doubly and singly bound oxygen (Fig. 1c–f).[20] The relative ratio of O singly or doubly bound to C follows a similar trend to the results obtained based on the C 1s XPS spectra. The minimal C/O ratio in the functionalized FLG here is 16.8, which is much higher as compared to GO with a C/O ratio typically in the range of 1.8–2.5.[17] This observation confirms the high quality of FLG after functionalization.

15446 | *J. Mater. Chem. A*, 2015, **3**, 15444–15450

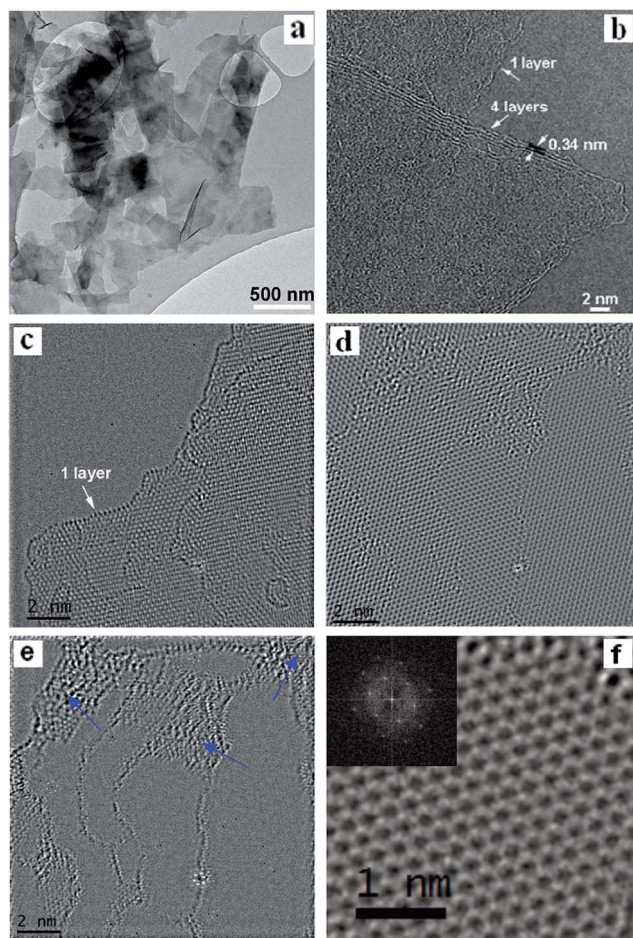This journal is © The Royal Society of Chemistry 2015

Fig. 3 (a) Wide-field TEM image of oxidised FLG. (b) TEM image of a monolayer stacked with a four-layer flake from an oxidised FLG sample. Aberration-corrected HRTEM images. (c) A pristine graphene monolayer. (d)–(f) Oxidised FLG. The arrows shown in image (e) point to the regions of amorphous carbon in image (d) which were high-lighted by masking and subtracting the crystalline graphene identified through the FFT from the image. The inset in (f) shows the FFT of the image. The oxidised FLG shown in (a, b and d–f) was obtained at 125 °C.
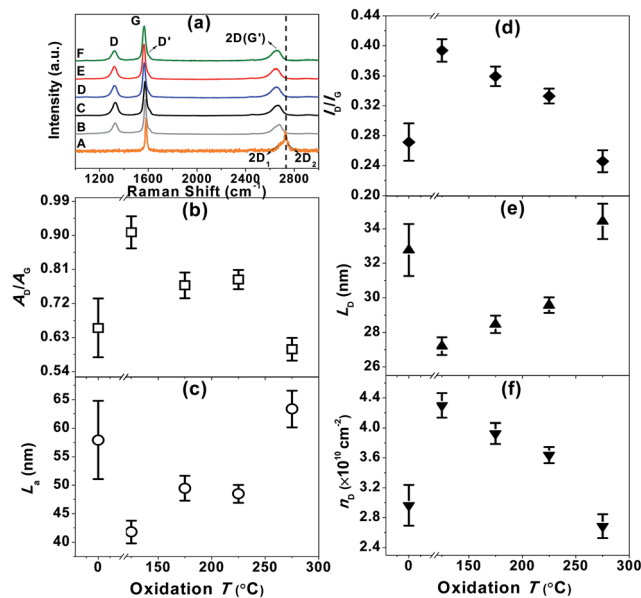

Fig. 4 (a) Raman spectra (633 nm excitation) of the starting graphite (trace A), FLG (trace B) and functionalized FLG (traces C–F). The spectra were normalized based on the G mode peak intensity. (b) A_D/A_G, (c) L_a, (d) I_D/I_G, (e) L_D and (f) n_D as a function of oxidation T.

Scanning electron microscopy (SEM) (Fig. 2) and transmission electron microscopy (TEM) (Fig. 3a) images show large quantities of graphene-like flakes. The edge-on HRTEM image of functionalized FLG (Fig. 3b) displays a characteristic inter-graphene spacing of 0.34 nm, in contrast to the double layer spacing of GO. An inspection of the HRTEM at high magnification shows the crystalline nature of both FLG (Fig. 3c) and OFLG consisting of an extended, two-dimensional sp^2 bound carbon "honeycomb" lattice (Fig. 3d and f and S3a†). Subtracting the crystalline structure from the image, by masking diffraction planes within the FFT, enables the amorphous carbon and defects to be clearly observed (Fig. 3e and S3b†).[19] The graphitic structure within the OFLG (Fig. 3d and f and S3a†) comprised up to approximately 75% of the area which suggests a substantial preservation of the original sp^2 bonding character. It is noted that, as opposed to most GO observed in literature,[22] holes were not seen in these OFLG.

Raman spectroscopy enabled us to study any generated defects. The Raman spectra of thin films prepared by filtering pristine– (trace B, Fig. 4a) and functionalized– (traces C–F, Fig. 4a) graphene dispersions all show an intense G band, a second-order two phonon mode 2D (also called G′) band and a disorder-related D peak. In stark contrast to the weak and broad 2D peak demonstrated for GO, the doublet 2D shape consisting of two components $2D_1$ and $2D_2$ typical of graphite, the 2D line for functionalized FLG here can be described as a single symmetrical Lorentzian peak in agreement with the Raman spectrum of randomly stacked flakes comprising fewer than 5 layers.[9–14] The defect level, as a function of oxidation temperature, was investigated in terms of the integrated Raman peak intensity (A_D/A_G) and the average peak intensity of the D band relative to the G band (I_D/I_G). It was found that A_D/A_G and I_D/I_G increased with oxidation temperature up to 125 °C beyond which both tended to decrease with temperature. Note that the maximum value of I_D/I_G is around 0.4 which is far less than that of GO ($I_D/I_G \approx 1.47$)[23] and high-quality reduced GO ($I_D/I_G \geq 0.5$).[24] Interestingly, the values of A_D/A_G and I_D/I_G for the FLG oxidised at 275 °C are both lower than those of pristine FLG, which may be due to the removal of some sp^3 defects by total oxidation. The in-plane crystallite size of graphene (L_a) was estimated based on the integrated area ratio of the D band and G band (A_D/A_G) using the equation $560(A_D/A_G)^{-1}/E^4$, where E is the laser energy (1.96 eV).[25] We found that L_a was first reduced upon treatment with HNO_3 vapour at 125 °C but started to rise with the increase of T. We further calculated the distance between defects (L_D), and the defect density of graphene (n_D) using the approximations of L_D^2 (nm^2) $= 4300(I_D/I_G)^{-1}/E^4$ and n_D (cm^{-2}) $= 10^{14}/\pi L_D^2$, respectively.[26] L_D showed a similar trend to L_a as a function of T. Though a prominent increase in n_D was

This journal is © The Royal Society of Chemistry 2015
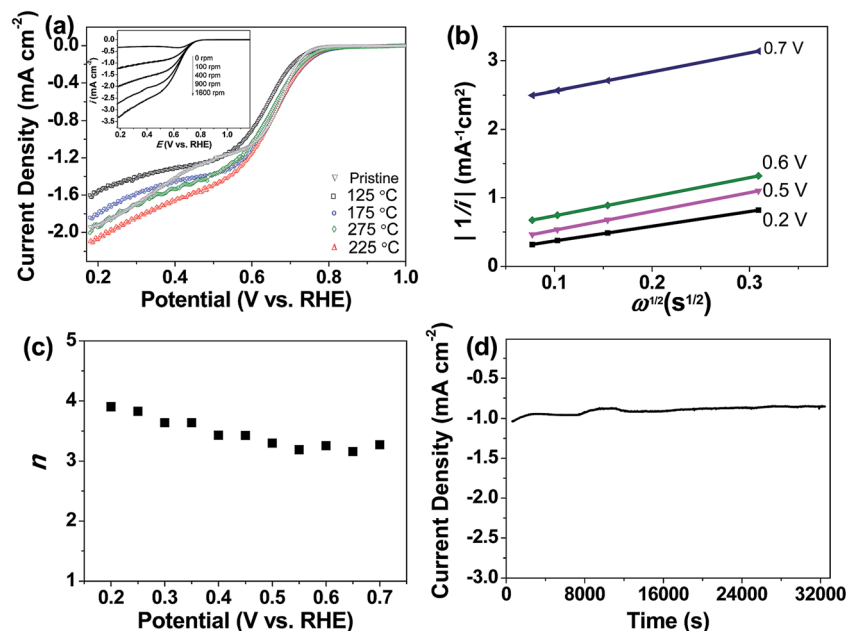
J. Mater. Chem. A, 2015, 3, 15444–15450 | 15447

Fig. 5 (a) Background corrected voltammograms recorded at 400 rpm and 10 mV s^{-1} in oxygen-saturated KOH (0.1 M) showing oxygen reduction by N-doped FLG pretreated with HNO$_3$ vapour at different temperatures. Inset: voltammograms recorded at different rotation speeds at a scan rate of 10 mV s^{-1} in oxygen-saturated KOH (0.1 M) for the N-doped FLG pretreated with HNO$_3$ vapour at 225 °C. (b) K−L plot extracted from the inset in (a). (c) Number of electrons transferred at different potentials. (d) Long-term chronoamperometric stability test at 0.6 V vs. RHE obtained at a rotation speed of 400 rpm in oxygen-saturated KOH (0.1 M).

observed for the functionalized FLG at 125 °C ($n_D = 4.3 \times 10^{10} \pm 1.6 \times 10^9$ cm^{-2}) compared to pristine FLG ($n_D = 3.0 \times 10^{10} \pm 2.7 \times 10^9$ cm^{-2}), the value fell gradually with further increase of T reaching $2.7 \times 10^{10} \pm 1.6 \times 10^9$ cm^{-2}, which is even lower than that of pristine FLG. Raman mapping of I_D/I_G over 25 regions (Fig. S4†) displays low defect densities of functionalized FLG with an overall large domain size. Given that the area occupied by a carbon atom in graphite is $(3^{3/2}/4)d^2$,[24,26] where d is the carbon–carbon bond length (0.1421 nm), the unperturbed domain size of the functionalized FLG at 125 °C is correlated to about 44 300 carbon atoms. This is three times larger than those (≤9900 carbon atoms) observed for chemically derived graphene.[24] These results strongly suggest the high quality of functionalized FLG produced using the approach proposed in this work.

Three steps are generally involved in the modified Hummers' method that is most commonly used for the preparation of GO.[27] Bulk graphite is first converted to a sulfuric acid–graphite intercalation compound, which is then transformed to pristine graphite oxide (PGO). In the end, GO is formed by the reaction of PGO with a solvent, involving the hydrolysis of covalent sulfates and loss of interlayer registry. In contrast to this conventional reaction pathway, here, the nitronium ion (NO$_2^+$) in nitric acid may initially attack the defect sites of the graphene surface, yielding a high concentration of hydroxyl or ether-type oxygen groups. This conjecture can be confirmed by the dominant C–O functional species derived from the C 1s spectra, being consistent with what has been observed for highly ordered pyrolytic graphite after treatment in 0.5 M HNO$_3$.[28] XPS results also suggested the presence of a small fraction of

carbonyls (most probably in ketones).[28] These carbonyls are formed where C–C bonds have been cleaved and can further convert into carboxyls and carboxylic anhydrides.[17] Based on the average OFLG flake size (Fig. 2a and 3a), the ratio of the edge carbon atoms to the basal plane atoms in the samples is ~1/200. Therefore, we conclude that some C–O and C═O atoms are located on the edges of vacancy defects in the basal planes.

We further demonstrated that the oxygen-functionalized FLG can also be modified with nitrogen upon exposure to NH$_3$, yielding a metal-free catalyst for the oxygen reduction reaction. XPS and EDX mapping during SEM observations confirmed the formation of nitrogen-containing groups in the sample (Fig. S5 and S6†). The N 1s region showed three nitrogen-functionalized carbon groups, namely pyridinic (398.6 eV, N$_1$), pyrrolic (399.8 eV, N$_2$), and quaternary (401.3 eV, N$_3$), respectively (Fig. S5 and S6†).[18,29] Evaluation of oxygen reduction by rotating disc electrode (RDE) voltammetry revealed that the N-doped FLG prepared by pretreatment with HNO$_3$ vapour at 225 °C exhibits significantly better performance, with a higher limiting current density but a lower onset potential than pristine FLG (Fig. 5a). This enhancement can be attributed to the presence of pyridinic N which reduces the adsorption energy of O$_2$, with graphitic N being able to promote the electro-reduction of O$_2$ to H$_2$O$_2$ via a two-electron pathway.[29,30] The onset potential is ≈0.755 V (vs. RHE), comparable to the value of 0.743 V (vs. RHE) reported for chemically synthesized N-graphene,[30] whilst the current densities at 0.7, 0.6, 0.5 and 0.2 V being approximately 0.4, 1.2, 1.5 and 2 mA cm^{-2}, respectively, are higher than those (≈0.2, 0.5, 0.9 and 1.3 mA cm^{-2} at 0.7, 0.6, 0.5 and 0.2 V, respectively) demonstrated for N-graphene.[30] We should point

15448 | J. Mater. Chem. A, 2015, 3, 15444–15450

This journal is © The Royal Society of Chemistry 2015

out that the N content in the sample is only 0.52 at%, much less than the N doping level (in the range of 3–5 at%) of graphene shown in literature.[30] The Koutecky–Levich (K–L) plots showed a linear relationship between $1/i$, $1/i_k$, and $1/w^{1/2}$ as follows:

$$\frac{1}{i} = \frac{1}{i_k} + \frac{1}{B\sqrt{\omega}}$$

where $B = 0.62nFAD^{2/3}\nu^{-1/6}C^*$, i and i_k are the measured and kinetic current respectively at a specific potential; n, the number of electrons transferred; D, the diffusion coefficient of the analyte, in this case O_2 (1.9×10^{-5} cm^2 s^{-1}); F, the Faraday constant (96 485 C mol^{-1}); A, the geometric area of the electrode (0.1256 cm^2); ν, the kinematic viscosity of the electrolyte (0.01 cm^2 s^{-1}), and C^* the solubility of oxygen in the electrolyte, which for the case of KOH (0.1 M) was taken to be 1.2×10^{-6} mole cm^{-3} (Fig. 5b).[29–32] The average number of electrons transferred during oxygen reduction on the basis of K–L analysis was found to slightly increase with overpotential, as depicted by the noticeable increase in the slope of the K–L lines from 0.2 V to 0.7 V (Fig. 5b), corresponding to 3.2 electrons at 0.75 V to 3.9 electrons at 0.2 V (Fig. 5c). The results indicate that oxygen reduction proceeds concurrently through both two sequential two-electron reactions with formation of OOH$^-$ intermediate, and through a direct four-electron reaction. Indeed, the features of the voltammograms are consistent with a series mechanism involving the reduction of oxygen to a peroxide intermediate at low overpotentials and its further reduction to OH$^-$ at higher potentials, as previously reported for N-doped graphene[29,30] and other metal-free catalysts.[18,31] Chemical disproportionation of the peroxide intermediate is also expected to proceed in parallel with its further electrochemical reduction, ultimately converting all the oxygen to OH$^-$.[30,31] Chronoamperometric measurements at 0.6 V showed no evident loss in activity after 8 h (Fig. 5d), indicating that the catalyst is able to sustain a stable performance over a long period of time.

4. Conclusions

In conclusion, we have developed a very simple and mild but effective gas-phase oxidation strategy using HNO_3 vapour for functionalization of graphene. XPS, HRTEM and Raman spectroscopy suggest the substantial preservation of the intrinsic properties of graphene after oxidation. The C/O ratio in the functionalized FLG (C/O ratio ~16.8) is much higher than GO with a C/O ratio typically in the range of 1.8–2.5. Controlling the oxidation temperature allows us to readily tune the surface oxygen functionalities. This strategy opens up a new route to produce high-quality oxidised few-layer graphene which can thus be used as a functional platform for advanced applications.

References

1 J. Malig, N. Jux and D. M. Guldi, *Acc. Chem. Res.*, 2013, **46**, 53–64.

2 A. Hirsch, J. M. Englert and F. Hauke, *Acc. Chem. Res.*, 2013, **46**, 87–96.

3 M. Quintana, E. Vazquez and M. Prato, *Acc. Chem. Res.*, 2013, **46**, 138–148.

4 M. B. C. Brodie, *Ann. Chim. Phys.*, 1855, **45**, 351–353.

5 D. C. Elias, R. R. Nair, T. M. G. Mohiuddin, S. V. Morozov, P. Blake, M. P. Halsall, A. C. Ferrari, D. W. Boukhvalov, M. I. Katsnelson, A. K. Geim and K. S. Novoselov, *Science*, 2009, **323**, 610–613.

6 J. R. Lomeda, C. D. Doyle, D. V. Kosynkin, W. F. Hwang and J. M. Tour, *J. Am. Chem. Soc.*, 2008, **130**, 16201–16206.

7 I. Gierz, C. Riedl, U. Starke, C. R. Ast and K. Kern, *Nano Lett.*, 2008, **8**, 4603–4607.

8 T. Ohta, A. Bostwick, T. Seyller, K. Horn and E. Rotenberg, *Science*, 2006, **313**, 951–954.

9 Y. Hernandez, V. Nicolosi, M. Lotya, F. M. Blighe, Z. Sun, S. De, I. T. McGovern, B. Holland, M. Byrne, Y. K. Gun'ko, J. J. Boland, P. Niraj, G. Duesberg, S. Krishnamurthy, R. Goodhue, J. Hutchison, V. Scardaci, A. C. Ferrari and J. N. Coleman, *Nat. Nanotechnol.*, 2008, **3**, 563–568.

10 Z. Y. Sun, X. Huang, F. Liu, X. N. Yang, C. Rösler, R. A. Fischer, M. Muhler and W. Schuhmann, *Chem. Commun.*, 2014, **50**, 10382–10385.

11 M. Lotya, Y. Hernandez, P. J. King, R. J. Smith, V. Nicolosi, L. S. Karlsson, F. M. Blighe, S. De, Z. M. Wang, I. T. McGovern, G. S. Duesberg and J. N. Coleman, *J. Am. Chem. Soc.*, 2009, **131**, 3611–3620.

12 Z. Y. Sun, J. Masa, Z. M. Liu, W. Schuhmann and M. Muhler, *Chem.–Eur. J.*, 2012, **18**, 6972–6978.

13 Z. Y. Sun, S. Pöller, X. Huang, D. Guschin, C. Taetz, P. Ebbinghaus, J. Masa, A. Erbe, A. Kilzer, W. Schuhmann and M. Muhler, *Carbon*, 2013, **64**, 288–294.

14 Z. Y. Sun, J. Vivekananthan, D. A. Guschin, X. Huang, V. Kuznetsov, P. Ebbinghaus, A. Sarfraz, M. Muhler and W. Schuhmann, *Chem.–Eur. J.*, 2014, **50**, 5752–5761.

15 F. Liu, J. Y. Choi and T. S. Seo, *Chem. Commun.*, 2010, **46**, 2844–2846.

16 W. S. Hummers and R. E. Offeman, *J. Am. Chem. Soc.*, 1958, **80**, 1339.

17 A. Dimiev, D. V. Kosynkin, L. B. Alemany, P. Chaguine and J. M. Tour, *J. Am. Chem. Soc.*, 2012, **134**, 2815–2822.

18 J. Masa, A. Q. Zhao, W. Xia, Z. Y. Sun, B. Mei, M. Muhler and W. Schuhmann, *Electrochem. Commun.*, 2013, **34**, 113–116.

19 A. W. Robertson, A. Bachmatiuk, Y. A. Wu, F. Schäffel, B. Rellinghaus, B. Büchner, M. H. Rümmeli and J. H. Warner, *ACS Nano*, 2011, **5**, 6610–6618.

20 W. Xia, C. Jin, S. Kundu and M. Muhler, *Carbon*, 2009, **47**, 919–922.

21 D. C. Marcano, D. V. Kosynkin, J. M. Berlin, A. Sinitskii, Z. Z. Sun, A. Slesarev, L. B. Alemany, W. Lu and J. M. Tour, *ACS Nano*, 2010, **4**, 4806–4814.

22 K. Erickson, R. Erni, Z. Lee, N. Alem, W. Gannett and A. Zettl, *Adv. Mater.*, 2010, **22**, 4467–4472.

23 J. Q. Liu, C. F. Chen, C. C. He, J. Zhao, X. J. Yang and H. L. Wang, *ACS Nano*, 2012, **6**, 8194–8202.

24 S. Eigler, M. Enzelberger-Heim, S. Grimm, P. Hofmann, W. Kroener, A. Geworski, C. Dotzer, M. Röckert, J. Xiao,

C. Papp, O. Lytken, H. P. Steinrück, P. Müller and A. Hirsch, *Adv. Mater.*, 2013, **25**, 3583–3587.

25 L. G. Cançado, K. Takai, T. Enoki, M. Endo, Y. A. Kim, H. Mizusaki, A. Jorio, L. N. Coelho, R. Magalhães-Paniago and M. A. Pimenta, *Appl. Phys. Lett.*, 2006, **88**, 163106.

26 L. G. Cançado, A. Jorio, E. H. M. Ferreira, F. Stavale, C. A. Achete, R. B. Capaz, M. V. O. Moutinho, A. Lombardo, T. S. Kulmala and A. C. Ferrari, *Nano Lett.*, 2011, **11**, 3190–3196.

27 A. M. Dimiev and J. M. Tour, *ACS Nano*, 2014, **8**, 3060–3068.

28 R. Burgess, C. Buono, P. R. Davies, R. J. Davies, T. Legge, A. Lai, R. Lewis, D. J. Morgan, N. Robinson and D. J. Willock, *J. Catal.*, 2015, **323**, 10–18.

29 L. F. Lai, J. R. Potts, D. Zhan, L. Wang, C. K. Poh, C. H. Tang, H. Gong, Z. X. Shen, J. Y. Lin and R. S. Ruoff, *Energy Environ. Sci.*, 2012, **5**, 7936–7942.

30 Y. Jiao, Y. Zheng, M. Jaroniec and S. Z. Qiao, *J. Am. Chem. Soc.*, 2014, **136**, 4394–4403.

31 J. Masa, A. Q. Zhao, W. Xia, M. Muhler and W. Schuhmann, *Electrochim. Acta*, 2014, **128**, 271–278.

32 L. M. Dai, Y. H. Xue, L. T. Qu, H. J. Choi and J. B. Baek, *Chem. Rev.*, 2015, DOI: 10.1021/cr5003563.